**Hydrology and
Earth System
Sciences**
Discussions

Open Access

Reconciling high altitude precipitation in the upper Indus Basin with glacier mass balances and runoff

W. W. Immerzeel[1,3], N. Wanders[1], A. F. Lutz[3], J. M. Shea[2], and M. F. P. Bierkens[1]

[1]Utrecht University, Department of Physical Geography, Heidelberglaan 2, P.O. Box 80115, Utrecht, the Netherlands
[2]International Centre for Integrated Mountain Development (ICIMOD), P.O. Box 3226, Kathmandu, Nepal
[3]FutureWater, Costerweg 1V, 6702 AA Wageningen, the Netherlands

Correspondence to: W. W. Immerzeel (w.w.immerzeel@uu.nl)

Discussion Paper | Discussion Paper | Discussion Paper | Discussion Paper

HESSD

12, 4755–4784, 2015

Inferring precipitation from glacier mass balances

W. W. Immerzeel et al.

Title Page

Abstract	Introduction
Conclusions	References
Tables	Figures

|◄   ►|

◄   ►

Back   Close

Full Screen / Esc

Printer-friendly Version

Interactive Discussion

Abstract

Mountain ranges in Asia are important water suppliers, especially if downstream climates are arid, water demands are high and glaciers are abundant. In such basins, the hydrological cycle depends heavily on high altitude precipitation. Yet direct observations of high altitude precipitation are lacking and satellite derived products are of insufficient resolution and quality to capture spatial variation and magnitude of mountain precipitation. Here we use glacier mass balances to inversely infer the high altitude precipitation in the upper Indus Basin and show that the amount of precipitation required to sustain the observed mass balances of the large glacier systems is far beyond what is observed at valley stations or estimated by gridded precipitation products. An independent validation with observed river flow confirms that the water balance can indeed only be closed when the high altitude precipitation is up to a factor ten higher than previously thought. We conclude that these findings alter the present understanding of high altitude hydrology and will have an important bearing on climate change impact studies, planning and design of hydropower plants and irrigation reservoirs and the regional geopolitical situation in general.

1 Introduction

Of all Asian basins that find their headwaters in the greater Himalayas, the Indus Basin depends most strongly on high altitude water resources (Immerzeel et al., 2010; Lutz et al., 2014). The largest glacier systems outside the polar regions are found in this area and the seasonal snow cover is the most extensive of all Asian basins (Immerzeel et al., 2009). In combination with a semi-arid downstream climate, a high demand for water owing to the largest irrigation scheme in the world and a large and quickly growing population, the importance of the upper Indus Basin (UIB) is evident (Immerzeel and Bierkens, 2012). The hydrology of the UIB ($4.37 \times 10^5\,\mathrm{km}^2$) is, however, poorly understood and the magnitude and distribution of high altitude precipitation is one of

its largest unknowns (Hewitt, 2005, 2007; Winiger et al., 2005; Ragettli and Pellicciotti, 2012; Immerzeel et al., 2013; Mishra, 2015). Annual precipitation patterns in the UIB result from the intricate interplay between synoptic scale circulation and valley scale topography-atmosphere interaction resulting in orographic precipitation and funnelling of air movement (Barros et al., 2004; Hewitt, 2013). At the synoptic scale, annual precipitation originates from two sources: the south-eastern monsoon during the summer and moisture transported by the westerly jet stream over central Asia (Scherler et al., 2011; Mölg et al., 2013) during winter. The relative contribution of westerly disturbances to the total annual precipitation increases from south-east to north-west, and the anomalous behaviour of Karakoram glaciers are commonly attributed to changes in winter precipitation (Scherler et al., 2011; Yao et al., 2012). At smaller scales the complex interaction between the valley topography and the atmosphere dictates the spatial distribution of precipitation (Bookhagen and Burbank, 2006; Immerzeel et al., 2014). Valley bottoms, where stations are located, are generally dry and precipitation increases up to a certain maximum altitude (HMAX) above which all moisture has been orographically forced out of the air and precipitation decreases again. In westerly dominated rainfall regimes HMAX is generally higher, which is likely related to the higher tropospheric altitude of the westerly airflow (Harper, 2003; Hewitt, 2005, 2007; Winiger et al., 2005; Scherler et al., 2011). Gridded precipitation products are the de facto standard in hydrological assessments, and they are either based on observations (e.g. APHRODITE; Yatagai et al., 2012), remote sensing (e.g. the Tropical Rainfall Monitoring Mission; Huffman et al., 2007) or reanalysis (e.g. ERA-Interim; Dee et al., 2011) (Fig. 1c to e). In most cases the station data strongly influence the distribution and magnitude of the precipitation in those data products, however the vast majority of the UIB is located at elevations far beyond the average station elevation (Fig. 1a and b). The few stations that are at elevations above 2000 m are located in dry valleys and we hypothesize that the high altitude precipitation is considerably underestimated (Fig. 1c–e). Moreover, remote sensing based products, such as TRMM, are insufficiently capable of capturing snowfall (Bookhagen and Burbank, 2006; Huffman

et al., 2007) and the spatial resolution (25 to 75 km^2) of most rainfall products (and the underlying models) is insufficient to capture topography-atmosphere interaction at the valley scale (Fig. 1c–e). Thus, there is a pressing need to improve the quantification of high altitude precipitation, preferably at large spatial extents and at high resolution.

5 Earlier work at the small scale suggested that the glacier mass balance may be used to reconstruct precipitation in its catchment area (Harper, 2003; Immerzeel et al., 2012b). Figure 1a and b shows that the glaciers are located at elevations that are in higher parts of the UIB, which are not covered by station data. Therefore the mass balances of the glaciers contain important information on high altitude accumulation in an area

10 that is inaccessible, ungauged, but very important from an hydrological point of view. In this study we further elaborate this approach by inversely modeling average annual precipitation from the mass balance of 550 large (> 5 km^2) glacier systems located throughout the UIB. We perform a rigorous uncertainty analysis and we validate our findings using independent observation of river runoff.

2   Methods

15

We use regionally-averaged glacier mass balance (MB) data from ICESat (Kääb et al., 2012) in combination with daily air temperature fields, a degree day melt model and a detailed elevation model to optimize the precipitation gradient (PG) so as to match the simulated and observed glacier mass balances. We apply geostatistical condi-

20 tional simulation (Goovaerts, 1997) to spatially interpolate the PG estimates to high-resolution PG fields, which are then used to estimate the high-altitude precipitation. To account for uncertainties in the estimated precipitation we randomly sample six critical parameters and generate 10 000 equiprobable precipitation fields and we validate our results using observed river runoff data.

2.1 Datasets

Glacier mass balance trends based on ICESat (Kääb et al., 2012) are recomputed for the period 2003 until 2008 for the three major mountain ranges in the UIB: the Karakoram, the Hindu-Kush and the Himalaya (Fig. 1). For each zone the mass balance is computed including a regional uncertainty estimate (Kääb et al., 2012). From the zonal uncertainty (σ_z) we estimate the SD between glaciers within a zone (σ_g) as

$$\sigma_g = \sigma_z \sqrt{n} \tag{1}$$

Where n is the number of glaciers within a zone. The σ_g values used in the uncertainty analysis are shown in Table 1.

Glacier outlines area based on the glacier inventory of the International Centre for Integrated Mountain Development (Bajracharya and Shrestha, 2011). We use runoff data and actual evapotranspiration (ETa) data for the validation of our results. For runoff we compiled all available published data, which we complemented with data made available by the Pakistan Meteorological Department and the Pakistan Water and Power Development Authority. To account for uncertainty in gridded ETa estimates we used four different products which we resampled to a 1 km^2 resolution at which we perform all our analysis:

- ERA-Interim reanalysis (Dee et al., 2011): ERA-Interim uses the HTESSEL land surface scheme (Dee et al., 2011) to compute actual evapotranspiration (ETa). For transpiration a distinction is made between high and low vegetation in the HTESSEL scheme and these are parameterized from the Global Land Cover Characteristics database at a nominal resolution of 1 km^2.

- MERRA reanalysis (Rienecker et al., 2011): the MERRA reanalysis product of NASA applies the state-of-the-art GEOS-5 data assimilation system that includes many modern observing systems in a climate framework. MERRA uses the GEOS-5 catchment LSM land surface scheme (Koster et al., 2000) to compute actual ET.

- ET-Look (Bastiaanssen et al., 2012): the ET-Look remote sensing model infers information on ET from combined optical and passive microwave sensors, which can observe the land-surface even under persistent overcast conditions. A two-layer Penman–Monteith forms the basis of quantifying soil and canopy evapo-ration. The dataset is available only for the year 2007, but it was scaled to the 2003–2007 average using the ratio between the 2003–2007 average and the 2007 annual ET based on ERA-INTERIM.

- PCRGLOB-WB (Wada et al., 2014): the global hydrological model PCRGLOB-WB computes actual evapotranspiration using potential evapotranspiration based on Penman–Monteith, which is further reduced based on available soil moisture.

The average annual ET for the period 2003–2007 for each of the four products is shown in Fig. 2. The spatial patterns show good agreement, but the magnitudes differ considerably. The average ET for the entire upper Indus equals $359 \pm 107\,\mathrm{mm\,yr^{-1}}$.

The daily APHRODITE precipitation (Yatagai et al., 2012) and air temperature datasets (Yasutomi et al., 2011) from 2003 until 2007 are used as reference datasets to ensure maximum temporal overlap with the ICESat based glacier mass balance dataset (Kääb et al., 2012). The precipitation dataset is resampled from the nominal resolution of $25\,\mathrm{km^2}$ to a resolution of $1\,\mathrm{km^2}$ using the nearest neighbour algorithm. The air temperature dataset is then bias-corrected using monthly linear regressions with independent station data to account for altitudinal and seasonal variations in air temperature lapse rates (Fig. 3).

2.2 Model description

We use the PC-Raster spatial–temporal modelling environment (Karssenberg et al., 2001) to model the mass balance of the major glaciers in each zone and subsequently estimate precipitation gradients required to sustain the observed mass balance. The model operates at a daily time step from 2003 until 2007 and a spatial resolution of $1\,\mathrm{km^2}$. For each time step the total accumulation and total melt are aggregated over

the entire glacier surface. Only glaciers with a surface area above $5\,km^2$ are included in the analysis (Karakoram = 232 glaciers, Hindu-Kush = 119, Himalaya = 204 glaciers) to avoid scale problems. The model is forced by the spatial precipitation and temperature fields. The precipitation fields are corrected using a precipitation gradient (PG, $\%\,m^{-1}$). Precipitation is positively lapsed using a PG between a reference elevation (HREF) to an elevation of maximum precipitation (HMAX). At elevations above HMAX the precipitation is negatively lapsed from its maximum at HMAX with the same PG. HREF and HMAX values are derived from literature (Table 1) including its uncertainty. HMAX varies per zone and lies at a lower elevation in the Himalayas than in the other two zones (Table 1). We spatially interpolate HMAX from the zonal values to cover the entire UIB. The melt is modelled over the glacier area using the positive degree day (PDD) method (Hock, 2005), with different degree day factors (DDF) for debris-covered (DDFd) and debris-free (DDFdf) glaciers derived from literature (Table 1). To account for uncertainty in DDF, the DDFd and DDFdf are taken into account separately in the uncertainty analysis. At temperatures below the critical temperature of $2\,^{\circ}C$ (Singh and Bengtsson, 2004; Immerzeel et al., 2013) precipitation falls in the form of snow and contributes to the accumulation. Avalanche nourishment of glaciers is a key contributor for UIB glaciers (Hewitt, 2005, 2011) and to take this process into account, we extend the glacier area with steep areas directly adjacent to the glacier with a slope over an average threshold slope (TS) of $0.2\,m\,m^{-1}$. This average threshold slope is derived by analyzing the slopes of all glacierised pixels in the basin (Fig. 4). To account for uncertainty in TS this parameter is taken into account in the uncertainty analysis.

For each glacier system we execute transient model runs from 2003 until 2007 and we compute the average annual mass balance from the total accumulation and melt over this period. We make two different runs for each glacier system with two different PGs ($0.3\,\%\,m^{-1}$ and $0.6\,\%\,m^{-1}$) and we use the simulated mass balances of these two runs and the observed mass balances based on ICESat to optimize the PG per glacier, such that the simulated mass balance matches the observed. To interpolate the glacier-specific PG-values to PG-fields we use geostatistical conditional simula-

tion (Goovaerts, 1997) with a standardized semi-variogram. In the semi-variogram, the nugget and the range are fixed and the sill is set equal to the variance of the PGs of all glaciers. The spatial PG fields are then used in combination with a digital elevation model to generate the corrected precipitation field.

2.3 Uncertainty analysis

A rigorous uncertainty analysis is performed to take into account the uncertainty in parameter values and uncertainty in regional patterns. To account for parameter uncertainty we perform a 10 000 member Monte Carlo simulation on the parameters given in Table 1. For each run we randomly sample the parameter space based on the average (μ) and the SD (σ), which are based on literature values. For the positively-valued parameters we use a log-Gaussian distribution and a Gaussian distribution in case parameter values can be negative. We take into account uncertainty in the following key parameters (HREF, HMAX, DDFd, DDFdg, TS) for the PG as well as uncertainty in the mass balance against which the PG is optimized (MB). Based on the results of the 10 000 simulations we derive the average corrected precipitation field and the associated uncertainty in the estimates.

To account for uncertainty in spatial correlation and the presence of spatial patterns in the parameters we perform a sensitivity analysis where we consider three cases:

– fully correlated: we assume the parameters are spatially fully correlated within a zone, e.g. for each of the 10 000 simulation a parameter has the same value within a zone;

– uncorrelated: we assume the parameters are spatially uncorrelated and within each zone each glacier system is assigned a random value;

– intermediate case: we use geostatistical unconditional simulation (Goovaerts, 1997) with a standardized semi-variogram (nugget = 0, sill = variance of parameter, range = 120 km).

Back | Close

Full Screen / Esc

Printer-friendly Version

Interactive Discussion

2.4 Validation

We estimate the average annual runoff (Q) for sub-basins in the UIB from

$$Q = P_{cor} - ET + MB \tag{2}$$

Where P_{cor} is the corrected average precipitation, ET is the average annual evapotranspiration based on the four products and MB is the glacier mass balance expressed over the sub-basin area. We then compare the estimated runoff values to the observed time series (Table 2).

3 Results and discussion

The average annual precipitation based on 10 000 conditionally simulated fields reveals a striking pattern of high altitude precipitation. The amount of precipitation required to sustain the large glacier systems is much higher than either the station observations or the gridded precipitation products imply. For the entire UIB the uncorrected average annual precipitation (Yatagai et al., 2012) for 2003–2007 is 437 mm yr^{-1} (191 km^3 yr^{-1}), an underestimation of more than 200 % compared with our corrected precipitation estimate of 913 ± 323 mm yr^{-1} (399 ± 141 km^3 yr^{-1}; Fig. 5). The greatest corrected annual precipitation totals in the UIB (1271 mm yr^{-1}) are observed in the elevation belt between 3750 to 4250 m compared to 403 mm yr^{-1} for the uncorrected case. In absolute terms the main water producing region is located in the elevation belt between 4250 and 4750 m where approximately 78 km^3 of rain and snow precipitates annually.

In the most extreme case, precipitation is underestimated by a factor 5 to 10 in the region where the Pamir, Karakorum and Hindu-Kush ranges intersect (Fig. 5). Our inverse modelling shows that the large glacier systems in the region can only be sustained if snowfall in their accumulation areas totals around 2000 mm yr^{-1} (Hewitt, 2007). This is in sharp contrast to precipitation amounts between 200 and 300 mm yr^{-1} that are reported by the gridded precipitation products (Fig. 1). Our results match well with the few

studies which are available. Annual accumulation values between 1000 and 3000 mm are reported for accumulation pits above 4000 m in the Karakoram (The Batura Glacier Investigation Group, 1979; Wake, 1989; Winiger et al., 2005). Our results show that the highest precipitation amounts are found along the monsoon-influenced southern Himalayan arc with values up to 3000 mm yr^{-1}, while north of the Himalayan range the precipitation decreases quickly towards a vast dry area in the north-eastern part of the UIB (Shyok sub-basin). In the north-western part of the UIB, westerly storm systems are expected to generate considerable amounts of precipitation at high altitude.

We estimated the uncertainty in the modelled precipitation field with the SD (σ) of the 10 000 realizations (Fig. 5). The signal to noise ratio is satisfactory in the entire domain, e.g. the σ is always considerably smaller than the average precipitation with an average coefficient of variation of 0.35. The largest absolute uncertainty is found along the Himalayan arc and this coincides with the precipitation pattern found here. Strikingly, the region where the underestimation of precipitation is largest, at the intersection of the three mountain ranges in the northern UIB, is also an area where the uncertainty is small even though precipitation gradients are large. By running a multiple regression analysis after optimizing the PGs we quantify the contribution of each parameter to the total uncertainty. The largest source of uncertainty in our estimate of UIB high altitude precipitation stems from the MB estimates, followed by the DDFdf, DDFd, TS, HREF and HMAX, although regional differences are considerable (Fig. 6). The MB constrains the precipitation gradients and thereby exerts a strong control on the corrected precipitation fields, in particular because the intra-zonal variation in MB is relatively large (Table 1). Thus, improved spatial monitoring techniques of the MB are expected to greatly improve precipitation estimates.

Figure 7 shows the result of uncertainty analysis associated to the spatial correlation of the parameters, which reveals that the impact on the average corrected precipitation is limited. Locally there are minor differences in the corrected precipitation amounts, but overall the magnitude and spatial patterns are similar. However, there are considerable differences in the uncertainty. The lowest uncertainty is found for the fully uncorrelated

Back | Close

Full Screen / Esc

Printer-friendly Version

Interactive Discussion

case, the fully correlated case has the highest uncertainty whereas the intermediate case is in between both. For the fully correlated case all glacier systems have the same parameter set for the specific realization and this results in a larger final uncertainty. In the uncorrelated case each glacier system has a different randomly sampled parameter set and this reduces the overall uncertainty as it spatially attenuates the variation in precipitation gradients.

The corrected precipitation is validated independently by a comparison to published average annual runoff data of 27 stations (Table 2). Runoff estimates based on the corrected precipitation agree well with the average observed annual runoff (Fig. 8). The runoff estimated for the uncorrected APHRODITE is consistently lower than the observed runoff, and in some occasions even negative. Runoff estimates were also made based on the ERA-INTERIM and TRMM precipitation products. The TRMM results yield a similar underestimation as the uncorrected APHRODITES product, but the runoff estimate based on the ERA-INTERIM precipitation agrees reasonably well with the observations. However the coarse resolution $(70\,\text{km}^2)$ (Fig. 1) is problematic and cannot be used to reproduce the mass balance (Fig. 9). Averaged over large catchments the precipitation may be applied for hydrological modeling, but at smaller scales there are likely very large biases. As a result, the observed glacier mass balances cannot be reproduced when the ERA-INTERIM dataset is used.

Our results reveal a strong relation between elevation and precipitation with a median PG for the entire upper Indus of $0.0989\,\%\,\text{m}^{-1}$, but with larger regional differences. Median precipitation gradients in the Hindu-Kush and Karakoram ranges $(0.260\,\%\,\text{m}^{-1}$ and $0.119\,\%\,\text{m}^{-1}$ respectively) are significantly larger than those observed in the Himalayan range, e.g $0.044\,\%\,\text{m}^{-1}$ (Fig. 10). In the Hindu-Kush, for example, for every $1000\,\text{m}$ elevation rise, precipitation increases by 260 % with respect to APHRODITE, which is based on valley floor precipitation. In combination with a higher HMAX in the Hindu-Kush and the Karakoram (e.g. $5500\,\text{m}$ vs. $4500\,\text{m}$ in the Himalayas; Winiger et al., 2005; Hewitt, 2007; Seko, 1987; Putkonen, 2004; Immerzeel et al., 2014) this suggests that westerly airflow indeed has a higher tropospheric altitude and that the interplay

between elevation and precipitation is stronger for this type of precipitation. Further research should thus focus on the use of high resolution cloud-resolving weather models (Mölg et al., 2013) for this region to further resolve seasonal topography-precipitation interaction at both synoptic and valley scales.

4   Conclusions

In this study we inversely model high altitude precipitation in the upper Indus Basins from glacier mass balance trends derived by remote sensing. Although there are significant uncertainties, our results unambiguously show that high altitude precipitation in this region is underestimated and that the large glaciers here can only be sustained if high altitude accumulation is much higher than most commonly used gridded data products.

Our results have an important bearing on water resources management studies in the region. The observed gap between precipitation and streamflow (Immerzeel et al., 2009) (with stream flow being larger) cannot be attributed to the observed glacier mass balance (Kääb et al., 2012), but is most likely the result of an underestimation of precipitation, as also follows from this study. With no apparent decreasing trends in precipitation (Archer and Fowler, 2004) the observed negative trends in stream flow in the glacierised parts of the UIB should thus be primarily attributed to decreased glacier and snow melt (Sharif et al., 2013) and increased glacier storage (Gardelle et al., 2012). In a recent study the notion of of negative trends in UIB runoff was contested and based on a recent analysis (1985–2010) it was concluded that runoff of Karakoram rivers is increasing (Mukhopadhyay and Khan, 2014a). The study suggests that increase glacier melt during summer is the underlying reason, which in combination with positive precipitation trends in summer does not contradict the neutral glacier mass balances in the region. From all of these studies it becomes apparent that precipitation is the key to understanding behavior of glacier and hydrology at large in the UIB. The precipitation we estimate in this study differs considerably, in magnitude and spatial distribution, from

datasets that are commonly used in design of reservoirs for hydropower and irrigation and as such it may have a significant impact and improve such planning processes.

The water resources of the Indus River play an important geopolitical role in the region, and our results could contribute to the provision of independent estimates of UIB precipitation. We conclude that the water resources in the UIB are even more important and abundant than previously thought. Most precipitation at high altitude is now stored in the glaciers, but when global warming persists and the runoff regime becomes more rain dominated, the downstream impacts of our findings will become more evident.

References

Archer, D.: Contrasting hydrological regimes in the upper Indus Basin, J. Hydrol., 274, 198–210, doi:10.1016/S0022-1694(02)00414-6, 2003. 4774

Archer, D.R. and Fowler, H.J.: Spatial and temporal variations in precipitation in the Upper Indus Basin, global teleconnections and hydrological implications, Hydrol. Earth Syst. Sci., 8, 47–61, doi:10.5194/hess-8-47-2004, 2004. 4766

Azam, M. F., Wagnon, P., Ramanathan, A., Vincent, C., Sharma, P., Arnaud, Y., Linda, A., Pottakkal, J. G., Chevallier, P., Singh, V. B., and Berthier, E.: From balance to imbalance:

a shift in the dynamic behaviour of Chhota Shigri glacier, western Himalaya, India, J. Glaciol., 58, 315–324, doi:10.3189/2012JoG11J123, 2012. 4773

Bajracharya, S. and Shrestha, B.: The Status of Glaciers in the Hindu Kush-Himalayan Region, Tech. rep., ICIMOD, Kathmandu, 2011. 4759

5   Barros, A. P., Kim, G., Williams, E., and Nesbitt, S. W.: Probing orographic controls in the Himalayas during the monsoon using satellite imagery, Nat. Hazards Earth Syst. Sci., 4, 29–51, doi:10.5194/nhess-4-29-2004, 2004. 4757

Bastiaanssen, W. G. M., Cheema, M. J. M., Immerzeel, W. W., Miltenburg, I. J., and Pelgrum, H.: Surface energy balance and actual evapotranspiration of the transboundary Indus Basin
10   estimated from satellite measurements and the ETLook model, Water Resour. Res., 48, W11512, doi:10.1029/2011WR010482, 2012. 4760

Bookhagen, B. and Burbank, D. W.: Topography, relief, and TRMM-derived rainfall variations along the Himalaya, Geophys. Res. Lett., 33, 1–5, doi:10.1029/2006GL026037, 2006. 4757

Dee, D. P., Uppala, S. M., Simmons, A. J., Berrisford, P., Poli, P., Kobayashi, S., Andrae, U.,
15   Balmaseda, M. A., Balsamo, G., Bauer, P., Bechtold, P., Beljaars, A. C. M., van de Berg, L., Bidlot, J., Bormann, N., Delsol, C., Dragani, R., Fuentes, M., Geer, A. J., Haimberger, L., Healy, S. B., Hersbach, H., Hólm, E. V., Isaksen, L., Kå llberg, P., Köhler, M., Matricardi, M., McNally, A. P., Monge-Sanz, B. M., Morcrette, J.-J., Park, B.-K., Peubey, C., de Rosnay, P., Tavolato, C., Thépaut, J.-N., and Vitart, F.: The ERA-Interim reanalysis: configuration and
20   performance of the data assimilation system, Q. J. Roy. Meteor. Soc., 137, 553–597, doi:10.1002/qj.828, 2011. 4757, 4759, 4775

Gardelle, J., Berthier, E., and Arnaud, Y.: Slight mass gain of Karakoram glaciers in the early twenty-first century, Nat. Geosci., 5, 322–325, doi:10.1038/ngeo1450, 2012. 4766

Goovaerts, P.: Geostatistics for Natural Resources Evaluation, Oxford University Press, New
25   York – Oxford, 1997. 4758, 4762

Hagg, W., Mayer, C., Lambrecht, A., and Helm, A.: Sub-debris melt rates on southern Inylchek Glacier, central Tian Shan, Geogr. Ann. A, 90, 55–63, doi:10.1111/j.1468-0459.2008.00333.x, 2008. 4773

Harper, J. T.: High altitude Himalayan climate inferred from glacial ice flux, Geophys. Res. Lett.,
30   30, 3–6, doi:10.1029/2003GL017329, 2003. 4757, 4758

Hewitt, K.: The Karakoram anomaly? Glacier expansion and the 'elevation effect,' Karakoram Himalaya, Mt. Res. Dev., 25, 332–340, doi:10.1659/0276-4741(2005)025[0332:TKAGEA]2.0.CO;2, 2005. 4757, 4761

Inferring precipitation from glacier mass balances

W. W. Immerzeel et al.

Title Page

Abstract	Introduction
Conclusions	References
Tables	Figures

◀◀   ▶▶

◀   ▶

Back   Close

Full Screen / Esc

Printer-friendly Version

Interactive Discussion

Hewitt, K.: Tributary glacier surges: an exceptional concentration at Panmah Glacier, Karakoram Himalaya, J. Glaciol., 53, 181–188, doi:10.3189/172756507782202829, 2007. 4757, 4763, 4765, 4773

Hewitt, K.: Glacier change, concentration, and elevation effects in the Karakoram Himalaya, upper Indus Basin, Mt. Res. Dev., 31, 188–200, doi:10.1659/MRD-JOURNAL-D-11-00020.1, 2011. 4761, 4773

Hewitt, K.: The regional context, in: Glaciers of the Karakoram Himalaya, chap. 1, Springer, Dordrecht, 1–33, doi:10.1007/978-94-007-6311-1, 2013. 4757

Hock, R.: Glacier melt: a review of processes and their modelling, Prog. Phys. Geog., 29, 362–391, doi:10.1191/0309133305pp453ra, 2005. 4761

Huffman, G. J., Adler, R. F., Bolvin, D. T., Gu, G., Nelkin, E. J., Bowman, K. P., Hong, Y., Stocker, E. F., and Wolff, D. B.: The TRMM Multisatellite Precipitation Analysis (TMPA): quasi-global, multiyear, combined-sensor precipitation estimates at fine scales, J. Hydrometeorol., 8, 38–55, doi:10.1175/JHM560.1, 2007. 4757, 4775

Immerzeel, W. W. and Bierkens, M. F. P.: Asia's water balance, Nat. Geosci., 5, 841–842, doi:10.1038/ngeo1643, 2012. 4756

Immerzeel, W., Droogers, P., De Jong, S. M., and Bierkens, M.: Large-scale monitoring of snow cover and runoff simulation in Himalayan river basins using remote sensing, Remote Sens. Environ., 113, 40–49, doi:10.1016/j.rse.2008.08.010, 2009. 4756, 4766

Immerzeel, W., Van Beek, L., and Bierkens, M.: Climate change will affect the Asian water towers, Science, 328, 1382–1385, doi:10.1126/science.1183188, 2010. 4756

Immerzeel, W., Beek, L. P. H., Konz, M., Shrestha, A. B., and Bierkens, M. F. P.: Hydrological response to climate change in a glacierized catchment in the Himalayas, Climatic Change, 110, 721–736, doi:10.1007/s10584-011-0143-4, 2012a. 4773

Immerzeel, W. W., Pellicciotti, F., and Shrestha, A. B.: Glaciers as a proxy to quantify the spatial distribution of precipitation in the Hunza Basin, Mt. Res. Dev., 32, 30–38, doi:10.1659/MRD-JOURNAL-D-11-00097.1, 2012b. 4758

Immerzeel, W., Pellicciotti, F., and Bierkens, M.: Rising river flows throughout the twenty-first century in two Himalayan glacierized watersheds, Nat. Geosci., 6, 742–745, doi:10.1038/NGEO1896, 2013. 4757, 4761, 4773

Immerzeel, W., Petersen, L., Ragettli, S., and Pellicciotti, F.: The importance of observed gradients of air temperature and precipitation for modeling runoff from a glacierised watershed in

the Nepalese Himalayas, Water Resour. Res., 50, 2212–2226, doi:10.1002/2013WR014506, 2014. 4757, 4765, 4773

Kääb, A., Berthier, E., Nuth, C., Gardelle, J., and Arnaud, Y.: Contrasting patterns of early twenty-first-century glacier mass change in the Himalayas, Nature, 488, 495–498, doi:10.1038/nature11324, 2012. 4758, 4759, 4760, 4766, 4773

Karssenberg, D., Burrough, P. A., Sluiter, R., and de Jong, K.: The PCRaster software and course materials for teaching numerical modelling in the environmental sciences, Transactions in GIS, 5, 99–110, doi:10.1111/1467-9671.00070, 2001. 4760

Khattak, M., Babel, M., and Sharif, M.: Hydro-meteorological trends in the upper Indus River Basin in Pakistan, Clim. Res., 46, 103–119, doi:10.3354/cr00957, 2011. 4774

Koster, R., Suarez, M., Ducharne, A., Stieglitz, M., and Kumar, P.: A catchment-based approach to modeling land surface processes in a general circulation model structure, J. Geophys. Res., 105, 24809–24822, 2000. 4759

Lutz, A. F., Immerzeel, W. W., Shrestha, A. B., and Bierkens, M. F. P.: Consistent increase in High Asia's runoff due to increasing glacier melt and precipitation, Nat. Clim. Change, 4, 1–6, doi:10.1038/NCLIMATE2237, 2014. 4756

Mihalcea, C., Mayer, C., Diolaiuti, G., Lambrecht, A., Smiraglia, C., and Tartari, G.: Ice ablation and meteorological conditions on the debris-covered area of Baltoro Glacier, Karakoram, Pakistan, Ann. Glaciol., 43, 292–300, 2006. 4773

Mishra, V.: Climatic uncertainty in Himalayan Water Towers, J. Geophys. Res.-Atmos., doi:10.1002/2014JD022650, in press, 2015. 4757

Mölg, T., Maussion, F., and Scherer, D.: Mid-latitude westerlies as a driver of glacier variability in monsoonal High Asia, Nat. Clim. Change, 4, 68–73, doi:10.1038/nclimate2055, 2013. 4757, 4766

Mukhopadhyay, B. and Khan, A.: Rising river flows and glacial mass balance in central Karakoram, J. Hydrol., 513, 191–203, 2014a. 4766

Mukhopadhyay, B. and Khan, A.: A quantitative assessment of the genetic sources of the hydrologic flow regimes in upper Indus Basin and its significance in a changing climate, J. Hydrol., 509, 549–572, doi:10.1016/j.jhydrol.2013.11.059, 2014b. 4774

Nicholson, L. and Benn, D.: Calculating ice melt beneath a debris layer using meteorological data, J. Glaciol., 52, 463–470, doi:10.3189/172756506781828584, 2006. 4773

Putkonen, J. K.: Continuous snow and rain data at 500 to 4400 m altitude near Annapurna, Nepal, 1991–2001, Arct. Antarct. Alp. Res., 36, 244–248, doi:10.1657/1523-0430(2004)036, 2004. 4765, 4773

Ragettli, S. and Pellicciotti, F.: Calibration of a physically based, spatially distributed hydrological model in a glacierized basin: on the use of knowledge from glaciometeorological processes to constrain model parameters, Water Resour. Res., 48, 1–20, doi:10.1029/2011WR010559, 2012. 4757

Rienecker, M. M., Suarez, M. J., Gelaro, R., Todling, R., Bacmeister, J., Liu, E., Bosilovich, M. G., Schubert, S. D., Takacs, L., Kim, G.-K., Bloom, S., Chen, J., Collins, D., Conaty, A., da Silva, A., Gu, W., Joiner, J., Koster, R. D., Lucchesi, R., Molod, A., Owens, T., Pawson, S., Pegion, P., Redder, C. R., Reichle, R., Robertson, F. R., Ruddick, A. G., Sienkiewicz, M., and Woollen, J.: MERRA: NASA's Modern-Era Retrospective Analysis for Research and Applications, J. Climate, 24, 3624–3648, doi:10.1175/JCLI-D-11-00015.1, 2011. 4759

Scherler, D., Bookhagen, B., and Strecker, M. R.: Spatially variable response of Himalayan glaciers to climate change affected by debris cover, Nat. Geosci., 4, 156–159, doi:10.1038/ngeo1068, 2011. 4757

Seko, K.: Seasonal variation of altitudinal dependence of precipitation in Langtang Valley, Nepal Himalayas, Bulletin of Glacier Research, 5, 41–47, 1987. 4765, 4773

Sharif, M., Archer, D. R., Fowler, H. J., and Forsythe, N.: Trends in timing and magnitude of flow in the Upper Indus Basin, Hydrol. Earth Syst. Sci., 17, 1503–1516, doi:10.5194/hess-17-1503-2013, 2013. 4766, 4774

Singh, P. and Bengtsson, L.: Hydrological sensitivity of a large Himalayan basin to climate change, Hydrol. Process., 18, 2363–2385, doi:10.1002/hyp.1468, 2004. 4761

The Batura Glacier Investigation Group: The Batura glacier in the Karakoram mountains and its variations, Sci. Sinica, 22, 958–974, 1979. 4764

Wada, Y., Wisser, D., and Bierkens, M. F. P.: Global modeling of withdrawal, allocation and consumptive use of surface water and groundwater resources, Earth Syst. Dynam., 5, 15–40, doi:10.5194/esd-5-15-2014, 2014. 4760

Wake, C.: Glaciochemical investigations as a tool to determine the spatial variation of snow accumulation in the central Karakoram, Northern Pakistan, Ann. Glaciol., 13, 279–284, 1989. 4764

Title Page

Abstract | Introduction

Conclusions | References

Tables | Figures

◄◄ | ►►

◄ | ►

Back | Close

Full Screen / Esc

Printer-friendly Version

Interactive Discussion

Winiger, M., Gumpert, M., and Yamout, H.: Karakorum-Hindukush-western Himalaya: assessing high-altitude water resources, Hydrol. Process., 19, 2329–2338, doi:10.1002/hyp.5887, 2005. 4757, 4764, 4765, 4773

Yao, T., Thompson, L., Yang, W., Yu, W., Gao, Y., Guo, X., Yang, X., Duan, K., Zhao, H., Xu, B., Pu, J., Lu, A., Xiang, Y., Kattel, D. B., and Joswiak, D.: Different glacier status with atmospheric circulations in Tibetan Plateau and surroundings, Nat. Clim. Change, 2, 663–667, doi:10.1038/nclimate1580, 2012. 4757

Yasutomi, N., Hamada, A., and Yatagai, A.: Development of a long-term daily gridded temperature dataset and its application to rain/snow discrimination of daily precipitation, Global Environ. Res., 3, 165–172, 2011. 4760, 4777

Yatagai, A., Yasutomi, N., Hamada, A., Kitoh, A., Kamiguchi, K., and Arakawa, O.: APHRODITE: constructing a long-term daily gridded precipitation dataset for Asia based on a dense network of rain gauges, Geophysical Research Abstracts, 14, 1401–1415, 2012. 4757, 4760, 4763, 4775

Table 1. Averages (μ) and SDs (σ) of predictors for the precipitation gradient. Values and ranges are based on literature as follows: HREF, HMAX: (Seko, 1987; Putkonen, 2004; Winiger et al., 2005; Hewitt, 2007, 2011; Immerzeel et al., 2012a, 2014), DDF_d, DDF_{df} (Mihalcea et al., 2006; Nicholson and Benn, 2006; Hagg et al., 2008; Azam et al., 2012; Immerzeel et al., 2013), MB (Kääb et al., 2012).

Variable	Acronym	Distribution	μ	σ
Reference elevation (m)	HREF	log-Gaussian	2500	500
Maximum elevation (m)	HMAX	log-Gaussian		
Himalayas			4500	500
Karakoram			5500	500
Hindu-Kush			5500	500
Degree day factor debris (mm$^\circ$C^{-1} day^{-1})	DDF_d	log-Gaussian	2	2
Degree day factor debris free (mm$^\circ$C^{-1} day^{-1})	DDF_{df}	log-Gaussian	7	2
Threshold slope (m m^{-1})	TS	log-Gaussian	0.2	0.05
Mass balance (m w.e. yr^{-1})	MB	Gaussian		
Himalayas			-0.49	0.57
Karakoram			-0.21	0.76
Hindu-Kush			-0.07	0.61

Table 2. Runoff stations used for validation. Catchment areas are delineated based on SRTM DEM.

Station	LAT	LON	Area (km^2)	Observed Q (m^3 s^{-1})	Period
Besham Qila[a]	34.906	72.866	198 741	2372.2	2003–2007
Tarbela inflow[a]	34.329	72.856	203 014	2370.3	2003–2007
Mangla inflow[a]	33.200	73.650	29 966	831.8	2003–2007
Marala inflow[a]	32.670	74.460	29 611	956.5	2003–2007
Dainyor bridge[a]	35.925	74.372	14 147	331.8	1966–2004
Skardu – Kachura[b]	35.435	75.468	146 200	1074.2	1970–2010
Partab Bridge[b]	35.767	74.597	177 622	1787.9	1962–2009
Yogo[b]	35.183	76.100	64 240	359.4	1973–2010
Kharmong[b]	34.933	76.217	70 875	452.3	1982–2010
Gilgit[b]	35.933	74.300	13 174	286.7	1980–2010
Doyian[b]	35.550	74.700	4000	135.7	1974–2009
Chitral[c]	35.867	71.783	12 824	271.9	1964–1996
Kalam[c]	35.467	72.600	2151	89.6	1961–1997
Naran[c]	34.900	73.650	1181	48.1	1960–1998
Alam bridge[b]	35.767	74.600	28 201	644.0	1966–2010
Chakdara[c]	34.650	72.017	5990	178.9	1961–1997
Karora[c]	34.900	72.767	586	21.2	1975–1996
Garhi Habibullah[c]	34.450	73.367	2493	101.8	1960–1998
Muzafferabad[c]	34.430	73.486	7604	357.0	1963–1995
Chinari[c]	34.158	73.831	14 248	330.0	1970–1995
Kohala[c]	34.095	73.499	25 820	828.0	1965–1995
Kotli[c]	33.525	73.890	2907	134.0	1960–1995
Shigar[b]	35.422	75.732	6681	202.6	1985–1998
Phulra[d]	34.317	73.083	1106	19.2	1969–1996
Daggar[d]	34.500	72.467	534	6.9	1969–1996
Warsak[e]	34.100	71.300	74 092	593.0	1967–2005
Shatial Bridge[b]	35.533	73.567	189 263	2083.2	1984–2009

[a]: Calculated based on discharge provided by the Pakistan Water and Power Development (WAPDA).
[b]: Based on Mukhopadhyay and Khan (2014b).
[c]: Based on Sharif et al. (2013).
[d]: Based on Archer (2003).
[e]: Based on Khattak et al. (2011).

Title Page

Abstract | Introduction

Conclusions | References

Tables | Figures

◄◄ | ►►

◄ | ►

Back | Close

Full Screen / Esc

Printer-friendly Version

Interactive Discussion
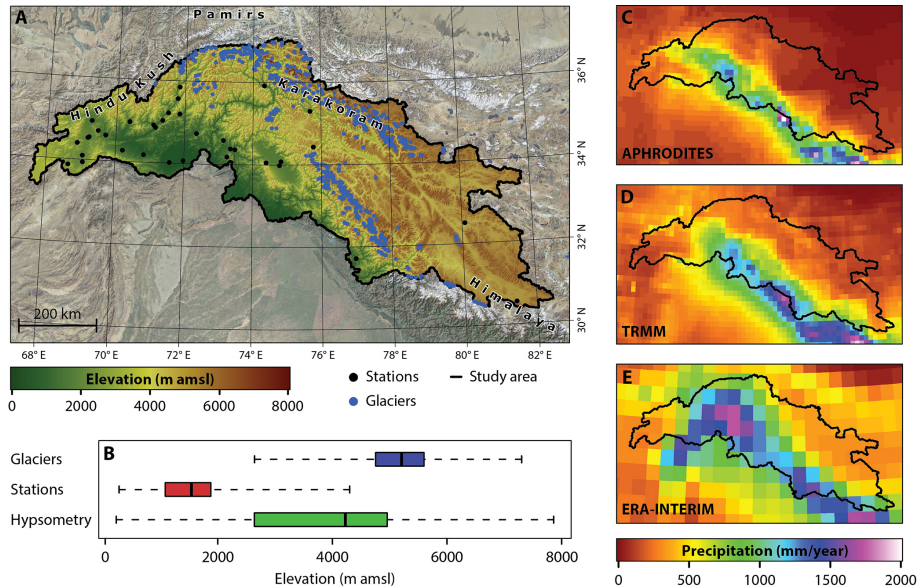
Figure 1. Overview of the UIB, basin hypsometry and three gridded precipitation products. **(a)** shows the digital elevation model and the location of the major glacier systems (area > 5 km^2) and the available stations in the Global Summary of the Day (GSOD) of the World Meteorological Organization (WMO). **(b)** shows boxplots of the elevation distribution of the basin, the large glacier systems and the GSOD stations. (**c** to **e**) show the average gridded annual precipitation between 1998–2007 for the APHRODITE (Yatagai et al., 2012), TRMM (Huffman et al., 2007) and ERA-INTERIM (Dee et al., 2011) datasets.
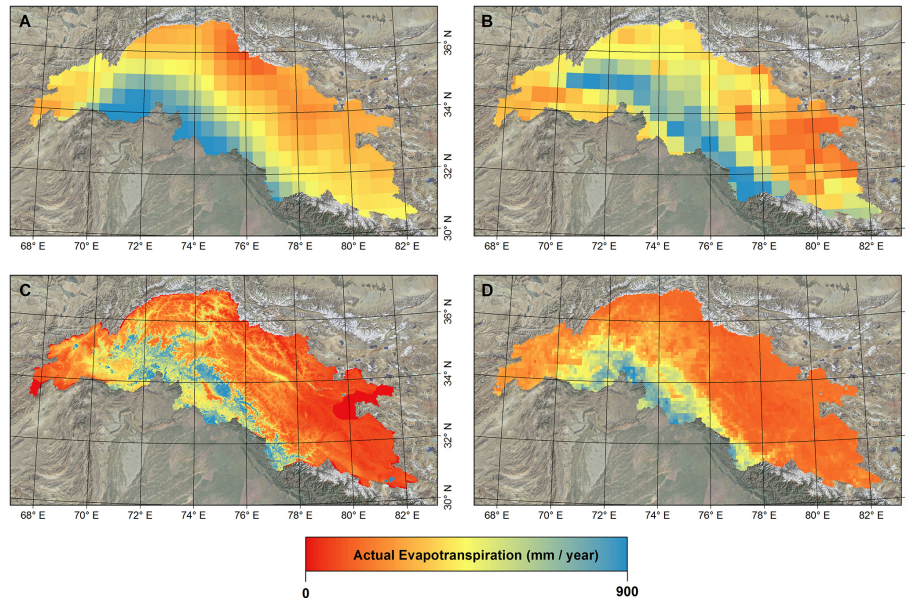
Figure 2. Average annual actual evapotranspiration between 2003 and 2007 for ERA-Interim **(a)**, MERRA **(b)**, ET-Look **(c)** and PCRGLOB-WB **(d)**.
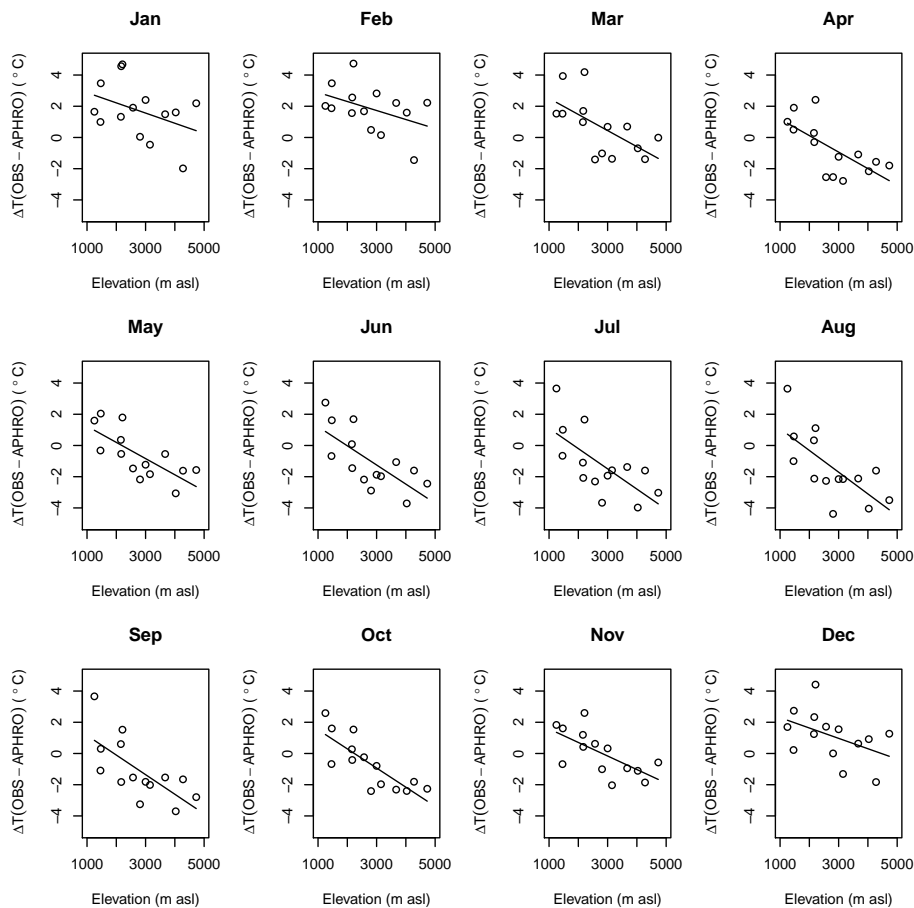
Figure 3. Monthly relation between observed temperatures at meteorological stations (OBS) and the APHRODITE temperature fields (APHRO) (Yasutomi et al., 2011).

Figure 4. Boxplots of slopes of glacierised areas per elevation bin.
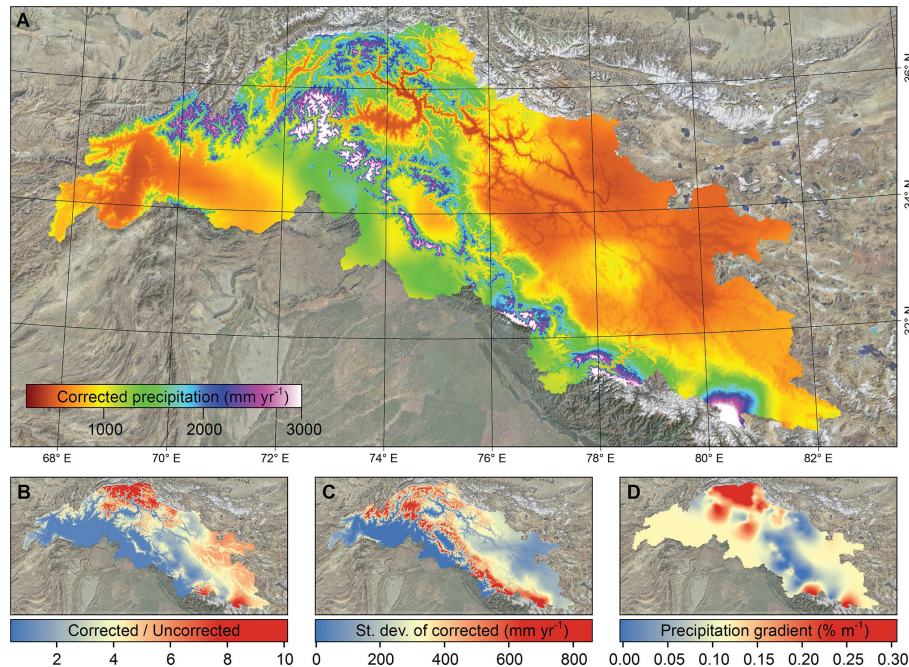
Figure 5. Corrected precipitation and estimated uncertainty for the UIB for the case with intermediate spatial correlation between model parameters. **(a)** shows the average modelled precipitation field based on 10 000 simulations for the period 2003–2007, **(b)** shows the ratio of corrected precipitation to the uncorrected APHRODITE precipitation for the same period, **(c)** shows the SD of the 10 000 simulations and **(d)** shows the average precipitation gradient.
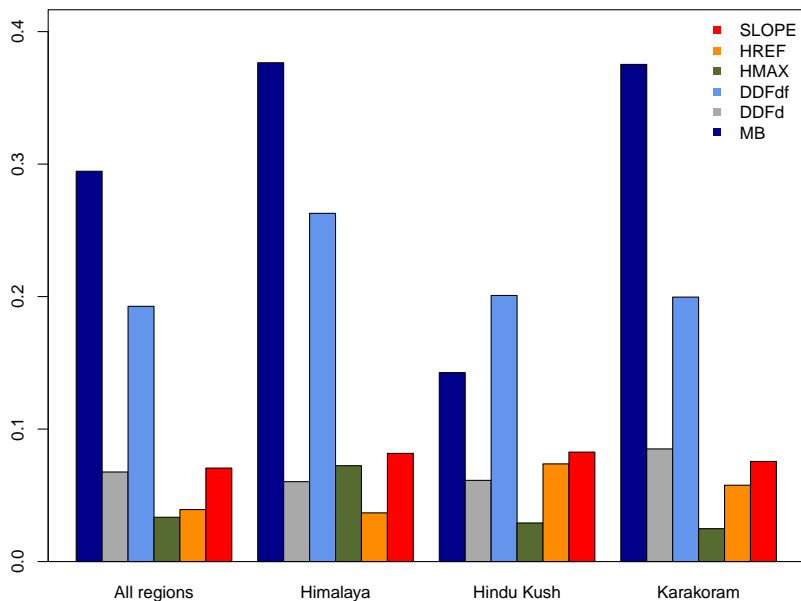
Figure 6. Normalized weights of multiple regression of the precipitation gradients by the predictors slope (slope threshold for avalanching to contribute to accumulation), HREF (base elevation from which lapsing starts), HMAX (elevation with peak precipitation), DDFd (degree day factor for debris covered glaciers), DDFdf (degree day factor for debris free glaciers) and the MB (mass balance of the glacier).
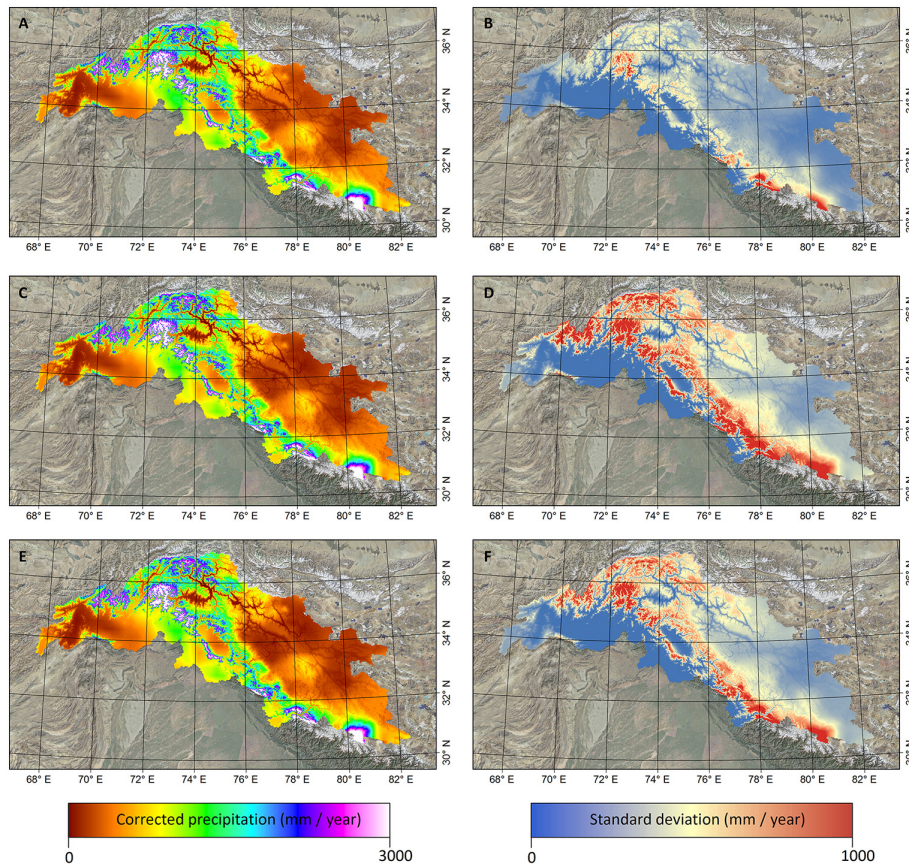
Figure 7. Impact of spatial correlation of parameters on the corrected precipitation field and associated uncertainty. The top panels show the corrected precipitation field **(a)** and uncertainty **(b)** for the fully uncorrelated case. The middle panels **(d, e)** for the fully correlated case and the bottom panels **(e, f)** for the intermediate case.

Full Screen / Esc

Printer-friendly Version

Interactive Discussion
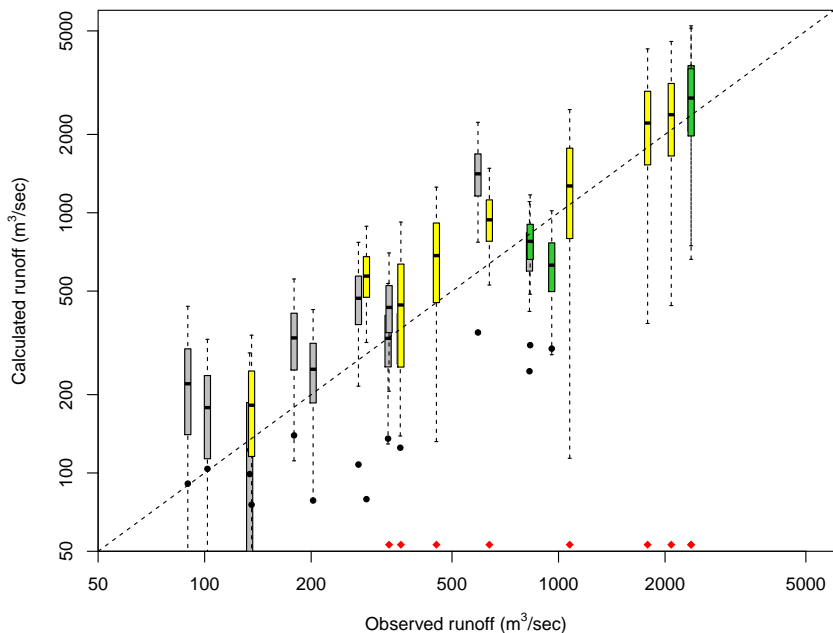
Figure 8. Validation of the precipitation correction using observed discharge (Table 2). The box plots are based on the runoff estimate based on 10 000 corrected precipitation fields (grey: stations for which the observed record does not coincide with the 2003–2007 period, yellow: stations for which the 2003–2007 period is part of the observational record, green: stations for which the observations are based precisely on the 2003–2007 period). The black dots and red diamonds (estimated runoff below $50\,\mathrm{m^3\,s^{-1}}$) show the estimated runoff based on the uncorrected precipitation.
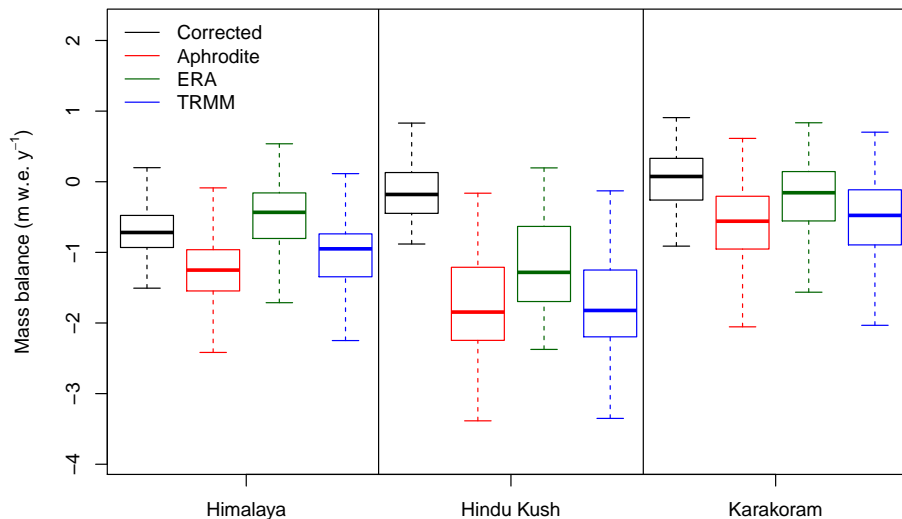
Figure 9. Reconstructed mass balances based on the corrected, APHRODITE, ERA-INTERIM and TRMM datasets. The black horizontal dotted line shows the observed mass balance for each zone.

Full Screen / Esc

Printer-friendly Version

Interactive Discussion
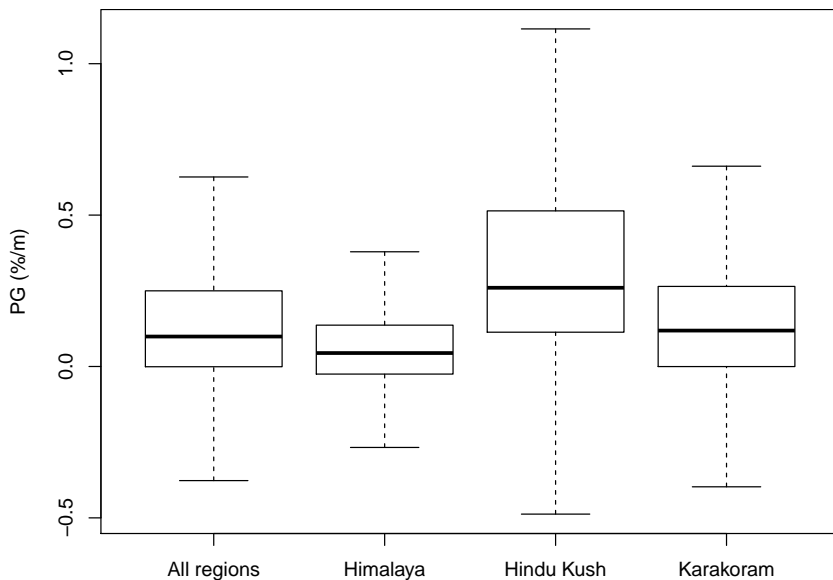
Figure 10. Box plots of precipitation gradients for the entire UIB and for the three regions separately